First-principles phase diagram calculations for the HfC–TiC, ZrC–TiC, and HfC–ZrC solid solutions

O. Adjaoud,[1,*,†] G. Steinle-Neumann,[1] B. P. Burton,[2] and A. van de Walle[3]
[1]*Bayerisches Geoinstitut, University of Bayreuth, 95440 Bayreuth, Germany*
[2]*Ceramics Division, Materials Science and Engineering Laboratory, National Institute of Standards and Technology, Gaithersburg, Maryland 20899-8520, USA*
[3]*Engineering and Applied Science Division, California Institute of Technology, Pasadena, California 91125, USA*
(Received 27 March 2009; revised manuscript received 3 August 2009; published 15 October 2009)

We report first-principles phase diagram calculations for the binary systems HfC–TiC, TiC–ZrC, and HfC–ZrC. Formation energies for superstructures of various bulk compositions were computed with a plane-wave pseudopotential method. They in turn were used as a basis for fitting cluster expansion Hamiltonians, both with and without approximations for excess vibrational free energies. Significant miscibility gaps are predicted for the systems TiC–ZrC and HfC–TiC, with consolute temperatures in excess of 2000 K. The HfC–ZrC system is predicted to be completely miscibile down to 185 K. Reductions in consolute temperature due to excess vibrational free energy are estimated to be ~7%, ~20%, and ~0%, for HfC–TiC, TiC–ZrC, and HfC–ZrC, respectively. Predicted miscibility gaps are symmetric for HfC–ZrC, almost symmetric for HfC–TiC and asymmetric for TiC–ZrC.

DOI: 10.1103/PhysRevB.80.134112 PACS number(s): 64.75.Nx, 61.43.−j, 61.66.Dk, 64.70.kd

I. INTRODUCTION

Transition metal carbides, including the NaCl-structured group IV (Ti, Zr, and Hf) carbides, have extremely high melting points and are therefore referred to collectively as the "refractory carbides." In addition to their high-temperature stabilities, these compounds exhibit interesting physical properties such as high hardnesses, high electrical conductivity, and superconductivity.[1] These properties make them suitable as bulk or thin-film materials in many technological applications: they are used as first-wall coatings for fusion reactors, protective coatings for cutting tools,[2] and low-friction coatings for bearings.[3] Their hardness is retained to very high temperature, and they have low chemical reactivity.[1,4] At room temperature, they are susceptible to attack only by concentrated acid or base in the presence of oxidizing agents, and retain good corrosion resistance to high temperature.[1,5,6] The transition-metal carbides have also been explored for a potential application as diffusion barriers in electronic devices.[7] Aside from the pure end members, solid solutions formed by these carbides are potentially of significant importance as properties can be optimized by varying the compositions in the binary—and higher order—systems.

Systematic experimental investigations of the phase diagrams and physical properties of such nonstoichiometric compounds are extremely challenging as many compositions need to be explored. The high melting points and limited solubilities of group IV carbides complicate experimental studies.[8–10] Phase diagram calculations allow one to establish the shape of the phase diagram with semiquantitative accuracy. Several semiempirical methods exist to construct phase diagrams based on approximate free-energy functions such as the model of subregular solutions[4,11,12] fitted to existing experimental data. Such thermodynamic models have also been applied to group IV carbides.[13–15]

Although these methods are useful to fit phase diagram data and approximate thermodynamic functions, it is desirable to compute phase diagrams strictly from knowledge of the constituent atoms without empirical parameters. To calculate phase equilibria the Gibbs free energy must be known for competing structures over a wide range of concentrations, and consequently the formation energy (ΔE_f) must be computed for a large number of phases along the solid solution.

At present, the three most widely employed approaches for this purpose can be summarized as follows. The most direct approach is the supercell method (e.g., Refs. 13 and 16–20), which is commonly employed to analyze local atomic structures and variations in bond lengths with chemical composition. The supercell method is based on the principle of spatial ergodicity, according to which all possible finite atomic arrangements are realized in a single infinite sample. This approach is computationally prohibitive when the size of the supercell is on the order of hundreds of atoms. In contrast to the supercell approach, methods based on perturbation theory perform the configurational average analytically. The most well-known approximation within alloy theory is the coherent-potential approximation (CPA) (e.g., Refs. 21–23). Recently it has also been demonstrated how short-range order effects can be incorporated in total-energy calculations using a nonlocal modification of the CPA.[23] Within the CPA-based methods no self-consistent calculation of elastic relaxation energies has been demonstrated to date, and such effects are generally treated using separate theoretical frameworks.[24–26] A third option is the cluster expansion (CE) approach.[27–31] It allows incorporating contributions to solid-solution energies arising from short-range order as well as elastic relaxations. In the CE method effective cluster interactions (ECIs) are fit to an extensive set of ΔE_f for supercells in the binary system, which is then explored to compute the phase diagram from Monte Carlo simulations. This approach is implemented in the alloy theoretic automated toolkit (ATAT) code,[32–34] which has successfully been applied to the study of phase stabilities in intermetallics, alloys, and pseudobinary systems (e.g., Refs. 35–40).

Here we explore by means of the CE method the subsolidus phase diagram of the binary refractory carbides HfC–

TiC, ZrC–TiC, and HfC–ZrC, by combining the ATAT package with *ab initio* total-energy calculations. We look in detail at the extent of miscibility between the phases and the consolute temperature (T_C) and composition (X_C). As experimental data and thermodynamic assessments of these systems are available[8–10,13,14] we compare predictions from the computations to measurements.

II. METHODOLOGY

Formation energies, ΔE_f, were calculated for transition-metal carbides HfC, TiC, and ZrC and many $M_m M'_n C_{(m+n)}$ supercells, in which M and M' are Hf, Ti, or Zr. All electronic structure calculations were performed with the Vienna *ab initio* simulation program (VASP),[41] using ultrasoft Vanderbilt-type pseudopotentials[42] with the generalized gradient approximation (GGA) for exchange and correlation.[43] Valence electron configurations for the pseudopotentials are Hf=$5p^6 6s^2 5d^2$, Ti=$3d^3 4s^1$, Zr=$4s^2 4p^6 5s^2 4d^2$, and C=$2s^2 2p^2$. Total energy calculations were converged with respect to k-point sampling, and a plane-wave energy cutoff of 500 eV was used which yields ΔE_f values that are converged to within a few meV per cation (Hf, Ti, and Zr). Cell constant and ionic positions were fully relaxed in all supercell computations.

Based on these results the first-principles phase diagram (FPPD) calculations were performed with the ATAT software package.[32–34] The ECI that define the CE are obtained by a least-squares fit of a subset of results for ΔE_f that are in turn used to predict ΔE_f of supercells computed in VASP but not included in the fit. The quality of the prediction is measured by the cross-validation score (CVS); unlike the traditional root-mean-square error, the CVS avoids overfitting the data, because it is able to detect the loss of predictive power resulting from an excessively large number of adjustable parameters in the fit. The optimal cluster sets were determined by minimizing the CVS between the *ab initio* computations and the CE prediction.[32]

Contributions of lattice vibrations (F_{vib}) to the free energies were approximated:[44] to reduce the computational burden of calculating phonon densities of states for a large set of superstructures, the bond-length-dependent transferable force-constant scheme[44] was employed. As discussed in Ref. 36 nearest-neighbor force constants were obtained for the end-members HfC, TiC, and ZrC as functions of imposed lattice parameters: in each system the lattice constants are varied between the end-member equilibrium, and forces are computed for five to six values. Depending on the variations in lattice constant this can lead to slightly different force constants for the same end member, e.g., HfC in the TiC–HfC and the HfC–ZrC systems.

The resulting bond stiffness versus bond-length relationships were applied to predict force constants for all superstructures, using the relaxed bond lengths and the chemical identities of bonds as predictors of their stiffness. The quantum-mechanical expression for the free energy was used, rather than the typical high-temperature (classical) limit. The resulting free energies were fit to temperature-dependent CE, which served as input for grand-canonical Monte Carlo simulations to calculate subsolidus phase diagrams.

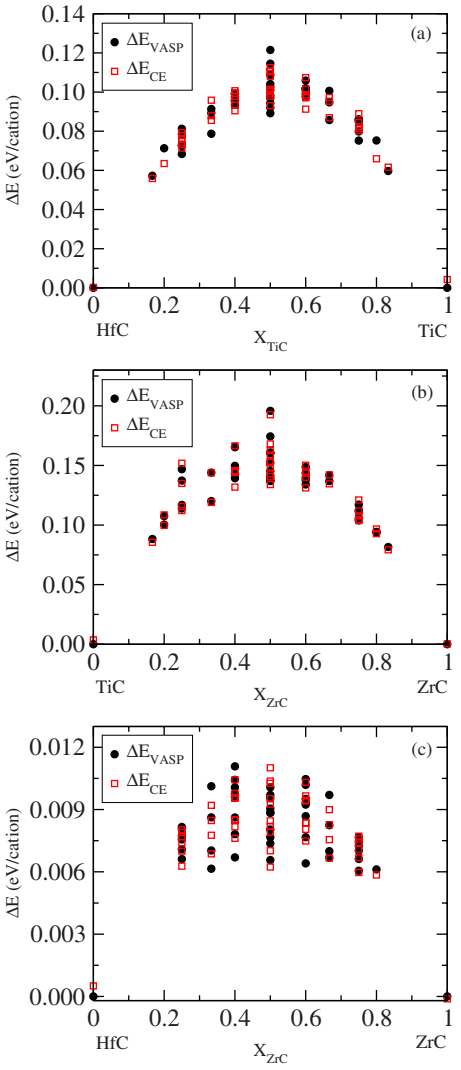

FIG. 1. (Color online) Formation energies, ΔE_f, for (a) $Hf_{1-x}Ti_xC$, (b) $Ti_{1-x}Zr_xC$, and (c) $Hf_{1-x}Zr_xC$ supercells. Closed circles are VASP results, and open squares are values calculated with cluster expansion Hamiltonians that were fit to VASP results.

III. RESULTS AND DISCUSSION

Figure 1 shows the static (0 K) ΔE_f from the *ab initio* computations that were used in fitting the CE Hamiltonians, and the corresponding formation energies predicted from the CEs. Formation energies of all the ordered structures are positive (Fig. 1). This is consistent with the experimental phase diagrams which exhibit no ordered intermediate compounds.[8,9] Formation energies for both the HfC–TiC and TiC–ZrC systems are of order 100 meV/cation, which is 1 order of magnitude larger than for HfC–ZrC. This suggests extensive miscibility gaps with high consolute temperatures for HfC–TiC and TiC–ZrC, comparable to AlN–InN.[37] Formation energies in HfC–ZrC are more like those in AlN–GaN,[37] i.e., consistent with complete miscibility at

TABLE I. Characteristics of the calculated cluster expansions.

Characteristics	HfC–TiC	TiC–ZrC	HfC–ZrC
Number of structures	45	41	49
Number of clusters	2+11+1	2+10+1	2+12
Cross-validation scores (meV/atom)	7.1	5.2	0.9

room temperature, also inferred from the thermodynamic assessment of the system.[14]

The CEs were fit to a moderate number of structures to obtain a good CVS (Table I). They include pair interactions only, or pair plus one triplet interaction (Table I and Fig. 2). Convergence of the effective cluster interactions (Fig. 2) is relatively fast, with pair interactions of less than the fifth-nearest-neighbor sufficient to obtain converged CEs. This contrasts with studies of metallic alloys, e.g., Al-TM (TM =Ti, Zr, and Hf) where interactions beyond the 10th neighbor shell are required,[40] and a large number of many-body (triplet and four-body) clusters need to be included. As expected, the ECIs exhibit a general trend of decreasing in amplitude with distance (Fig. 2), except for a significant negative value at four times the nearest-neighbor distance. This corresponds to ordering of cations of the same type on second-neighbor sites along the cell edges. For all three systems, the resulting CVS is significantly below 10 meV/atom, i.e., a small fraction of the formation energies.[32] We have explored different CEs with additional structures to explore the ECI behavior at four times the nearest-neighbor distance and found the feature to be robust. The presence of three-body terms (Table I) in the CE Hamiltonians for HfC–TiC and TiC–ZrC implies asymmetric immiscibility in these systems.

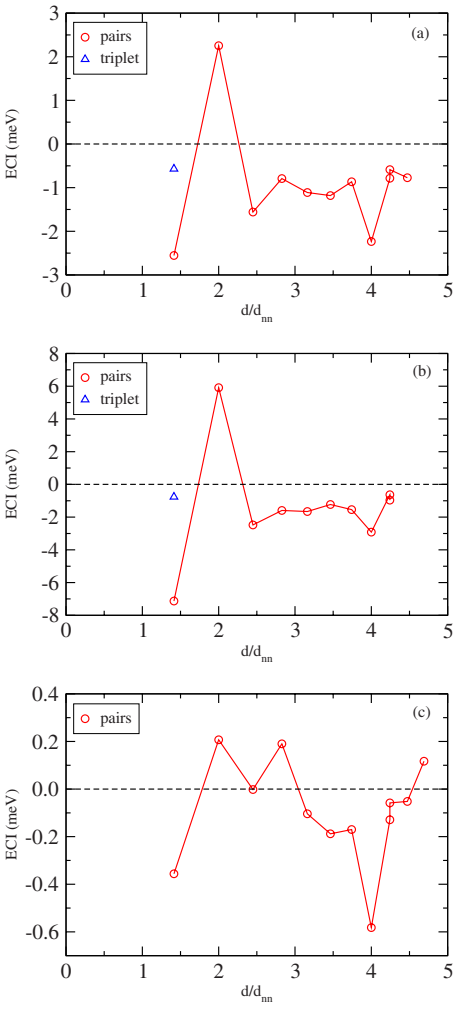

FIG. 2. (Color online) Calculated ECIs as functions of cluster diameter (normalized to nearest-neighbor distance) in (a) HfC–TiC, (b) TiC–ZrC, and (c) HfC–ZrC.

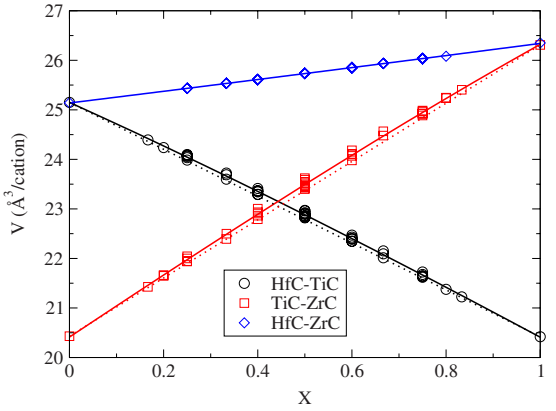

FIG. 3. (Color online) Cluster expansion fits (solid lines) and VASP supercell calculations of volume as functions of composition for HfC–TiC, TiC–ZrC, and HfC–ZrC. The dashed lines connect end points for supercell calculations, defining ideal mixing.

Figure 3 shows volumes as functions of bulk composition from the cluster expansion. Trends for all three systems are close to linear—Vegard's law—with a fit for HfC–ZrC that is within computational error of ideal mixing. Positive deviations from ideality are predicted for HfC–TiC and TiC–ZrC. Excess volumes of mixing in these systems imply immiscibilities that would persist under pressure. In contrast, immiscibility with negative volumes of mixing, as in the wurtzite-structured nitrides,[37] implies decreased immiscibility under pressure.

The dependence of the stretching and bending force constants on bond length are shown in Fig. 4. Stretching constants decrease monotonically with increasing bond length; bending terms, by contrast, are relatively insensitive. The Ti-C stretching and bending constants in HfC–TiC and TiC–ZrC plot as a single curve. Thus, Ti-C force constants are transferable between the HfC–TiC and TiC–ZrC systems. This effect was also predicted for Au-Cu, Au-Pd, and Cu-Pd systems.[45] In the Al-TM systems, however, the Al-Al bond force constants exhibited significant differences in the Al-Ti, Al-Zr, and Al-Hf systems.[39]

Subsolidus phase diagrams of the binary systems are computed with and without F_{vib}(Fig. 5). As expected from the presence of three-body terms in the ECIs for HfC–TiC and TiC–ZrC (Table I and Fig. 2) the corresponding phase diagrams are asymmetric.

The system HfC–TiC exhibits almost complete immiscibility below ~750 K and there is slight asymmetry with

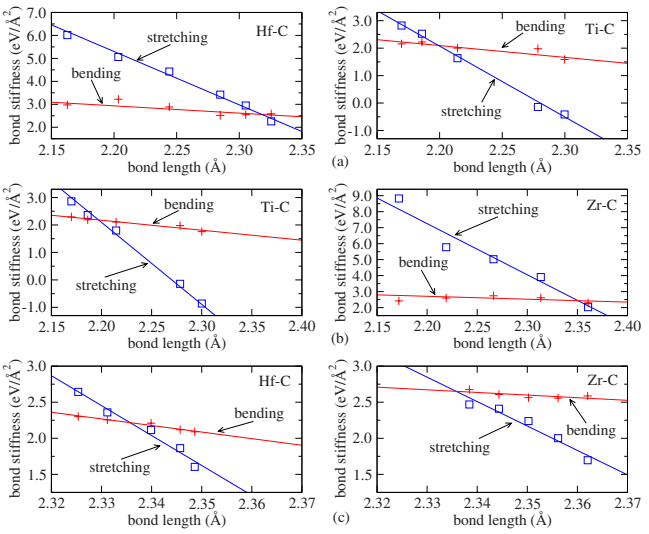

FIG. 4. (Color online) Nearest neighbor stretching and bending force constants versus bond length in (a) HfC–TiC, (b) TiC–ZrC, and (c) HfC–ZrC. Squares (blue) and crosses (red) indicate *ab initio* data points, and lines are linear fits used in the calculations of the vibrational free energy.

greater solubility on the HfC (larger-cation) side (Fig. 5). The consolute composition, however, is at X_C=0.50 (Table II). Experimental data[8,9] and their thermodynamic assessment,[14] even when combined with *ab initio* computations on ordered intermediate compounds,[13] exhibit stronger asymmetry. In HfC–TiC, including vibrational contributions to the free energy reduces T_C by about 7% from 2275 to 2120 K, within the uncertainty of experimental values[8,9] (Table II).

The TiC-ZrC system exhibits greater asymmetry, with higher solubility (Fig. 5) on the larger-cation (ZrC) side[46] (Fig. 3). Without taking F_{vib} into account we calculate X_C =0.5, but with F_{vib} it shifts to X_C=0.41, in good agreement with experimental work[9] and thermodynamic modeling[13,14] (Table II). By including F_{vib} the consolute temperature is reduced from 3350 to 2695 K (~20%). This reduction is large relative to most alloy systems (e.g., 5–15 %),[44] but significantly smaller than the ~43% reduction reported for the NaCl-KCl system.[36] T_C, however, is still considerably higher than experimental and thermodynamic values that yield 2250 K$\leq T_C \leq$2400 K (Table II). Our computations exhibit nearly complete immiscibility below ~1000 K, in agreement with experiments.[8,10]

In the absence of three-body terms in the HfC–ZrC ECI the Monte Carlo simulations yield a symmetric phase diagram (Fig. 5). As expected from the low formation energies (Fig. 1) we obtain T_C=185 K (Table II), consistent with thermodynamic data.[14] The low T_C can also be understood in terms of the small difference in equilibrium volume across the solid solution (Fig. 3) or the almost identical cation radii of Hf (0.71 Å) and Zr (0.72 Å).[46]

Consolute temperature differences between the carbide solid solutions can also be rationalized in terms of cation radii, or more specifically the differences in radii of the interchangeable cation: $\%\Delta R_{ij}=200|R_i-R_j|/(R_i+R_j)$ (Fig. 6). The mismatch is largest in TiC-ZrC and almost nonexistent

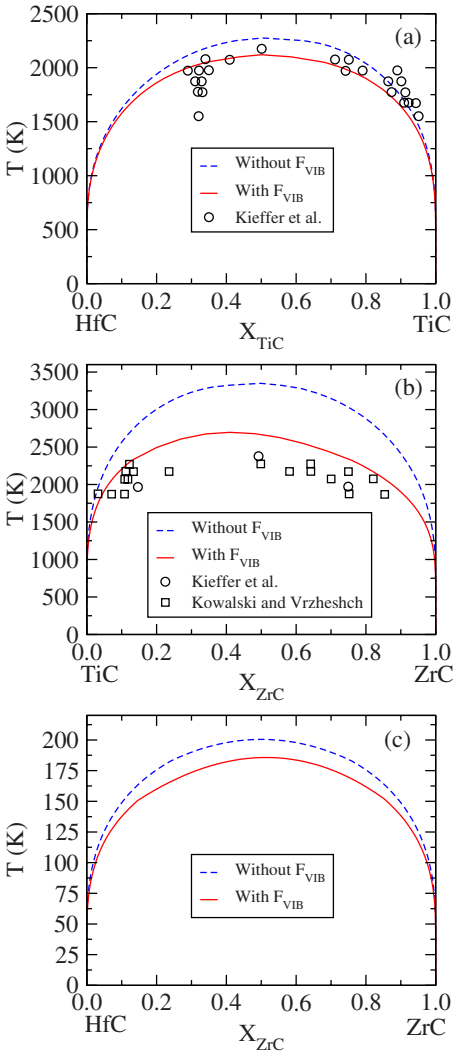

FIG. 5. (Color online) Calculated phase diagrams for the systems: (a) HfC–TiC, (b) TiC–ZrC, and (c) HfC–ZrC. Dashed (blue) curves are for calculations that did not include F_{vib}, and solid (red) curves are for calculations that did. Experimental data are from Ref. 8 (circles) and Ref. 10 (squares).

in HfC–ZrC, corresponding to the largest and smallest T_C, respectively. This suggests that immiscibility in group IV carbides is caused by ionic size effects. Similarly, larger values for $\%\Delta R_{ij}$ yield larger reductions in T_C (ΔT_C) induced by F_{vib}. As a consequence, the highest ΔT_C occurs in the system with the largest T_C. This is in contrast to the wurtzite-structured nitrides[37] in which T_C reductions due to F_{vib} anti-correlate with $\%\Delta R_{ij}$.

Considerations of elastic energy provide an alternative way to asses the energetics of cation substitutions and rationalizing the asymmetries of phase diagrams. Here we compute the elastic energy by the $\epsilon-G$ approximation[47–50] for the three binary systems: The equations of state of end-members HfC, TiC, and ZrC are computed, i.e., $E(V)$ where the volume of the cell for the end members are varied and then transformed to $E(X)$ via the CE volumes (Fig. 3). Finally, $\Delta E(X)$ is approximated by a linear combination of end-member equations of state (e.g., for HfC–TiC, $\Delta E(X)=(1-X)E_{\mathrm{HfC}}(X)+XE_{\mathrm{TiC}}(X)$). The resulting $\Delta E(X)$ for HfC–ZrC

TABLE II. Calculated consolute points.

System method	Without $F_{vib}\{X_C, T_C(K)\}$	With F_{vib} $\{X_C, T_C(K)\}$	Method references
HfC–TiC	0.50,2275	0.50, 2120	FPPD[a]
		0.55, 2133	Exp.[b]
		0.55, 2053	Exp.[c]
		0.60, 2173	SE[d]
		0.56, 2075	SR[e]
TiC-ZrC	0.50,3350	0.41, 2695	FPPD[a]
		0.45, 2273	Exp.[b]
		0.45, 2373	SE[d]
		0.35, 2281	SR[e]
HfC–ZrC	0.50, 200	0.50, 185	FPPD[a]
		–, <300	SR[e]

[a]FPPD=First-principles phase diagram; this work.
[b]Experimental results from Kieffer *et al.* (Ref. 8).
[c]Experimental results from Rogl *et al.*(Ref. 9).
[d]SE=Combined CALPHAD modeling with experimental data and *ab initio* results from Markström *et al.*(Ref. 13).
[e]SR=Subregular model from Gusev (Ref. 14).

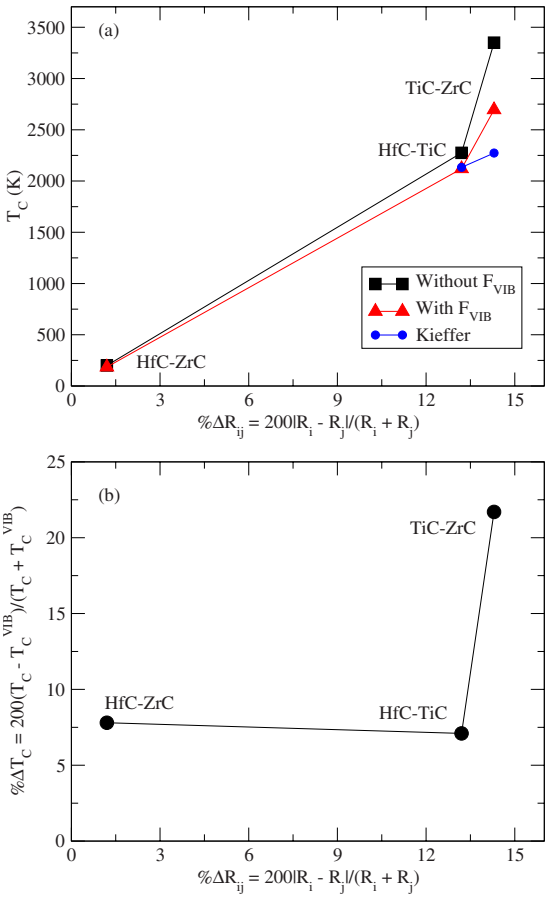

FIG. 6. (a) (Color online) Variation in the consolute temperature T_C as a function of the percentage difference in the ionic radii of exchangeable ions from the calculations with (triangles) and without F_{vib} (squares). Experimental data are included from Refs. 8 and 9. (b) Related percentage reduction in T_C from including F_{vib} in the cluster expansion Hamiltonian.

is symmetric (Fig. 7), for HfC–TiC and TiC–ZrC it is asymmetric with mixima closer to the end member with the smaller ion[46] (Fig. 7). This implies that more energy is required to replace a smaller ion with a larger one than vice versa and that the deviation of X_C from 0.5 is directly correlated with the difference in cation radii (Fig. 6). This is consistent with the wurtzite-structured nitrides,[37] and the quasibinary system TiC-ZrC.[50]

IV. CONCLUSIONS

First-principles phase diagram calculations for the binary systems HfC–TiC, TiC–ZrC, and HfC–ZrC predict miscibility gaps with consolute temperatures, T_C=2120, 2695, and 185 K, respectively. Including F_{vib} reduces T_C by ~7%,

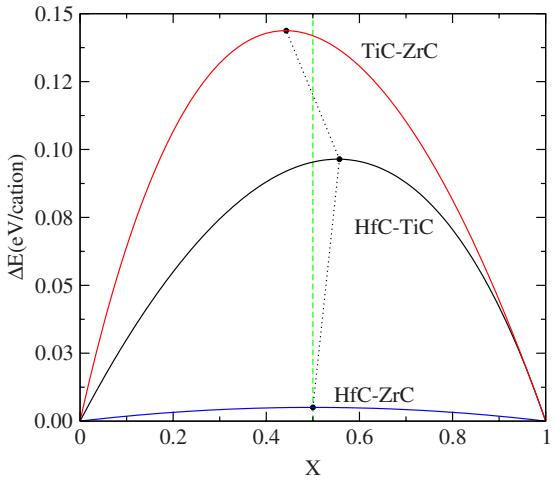

FIG. 7. (Color online) Elastic energy estimated by the ϵ–G approximation for the systems HfC–TiC, TiC–ZrC, and HfC–ZrC. The dotted line connects the maxima.

~20%, and ~0% for these systems, respectively. In the TiC-ZrC system the F_{vib}-effect is large relative to most alloy systems,[44] but significantly smaller than the ~43% effect reported for NaCl-KCl.[36] Miscibility gaps are predicted for all three binaries with an approximately symmetric phase diagram for HfC–TiC, a symmetric phase diagram for HfC–ZrC, and an asymmetric phase diagram for TiC–ZrC. Extensive immiscibility in the systems with high consolute temperatures (HfC–TiC and TiC–ZrC) limits optimization of material properties through ionic substitutions. For the carbide binary solid solutions the degree of miscibility and T_C are directly correlated with differences in ionic radii of the exchangeable cations, with larger ions more readily replaced by smaller ones than vice a versa.

ACKNOWLEDGMENTS

This work was in part supported by the Graduate School "Oxides" in the Elite Netzwerk Bayern, funded by the State of Bavaria. The collaboration between GSN and AvdW has been supported by the Bavaria California Technology Center (BaCaTeC). A.v.d.W. was supported by the U.S. National Science Foundation through TeraGrid resources provided by NCSA and SDSC under Grant No. TG-DMR050013N and by the U.S. Department of Energy National Nuclear Security Administration under Grant No.DE-FC52-08NA28613. We greatly appreciate helpful discussion with David Dolejš, Dan Frost, and Nico de Koker.

*adjaoud@gfz-potsdam.de
†Present address: GFZ German Research Centre for Geosciences, Section 3.3, Telegrafenberg, 14473 Potsdam, Germany.

[1] L. E. Toth, *Transition Metal Carbides and Nitrides* (Academic Press, New York, 1971).
[2] P. Schwarzkopf, R. Kieffer, W. Leszynski, and F. Benesovsky, *Refractory Hard Metals* (Macmillan, New York, 1953).
[3] *Refractory Carbides*, edited by G. V. Samronov (Consultants Bureau, New York, 1974).
[4] E. K. Storms, *The Refractory Carbides* (Academic Press, New York, 1967).
[5] S. T. Oyama, *The Chemistry of Transition Metal Carbides and Nitrides* (Blackie Academic and Professional, Glasgow, 1996).
[6] H. O. Pierson, *Handbook of Refractory Carbides and Nitrides, Noyes Publications* (Westwood, Massachusetts, 1996).
[7] H.-Y. Tsai, S.-C. Sun, and S.-J. Wang, J. Electrochem. Soc. **147**, 2766 (2000).
[8] R. Kieffer, H. Nowotny, A. Neclcel, P. Ettmayer, and L. Usner, Monatsh. Chem. **99**, 1020 (1968); R. Kieffer and P. Ettmayer, Angew. Chem., Int. Ed. **9**, 926 (1970).
[9] P. Rogl, S. K. Naik, and E. Rudy, Monatsh. Chem. **108**, 1189 (1977).
[10] A. E. Kowalskii and E. Ya. Vrzheshch, in *Hard Metals Production Technology and Research in the USSR*, edited by S. J. Bashkirov (Pergamon Press, New York, 1964).
[11] J. L. Murray, in *Phase Diagrams of Binary Titanium Alloys*, edited by J. L. Murray (ASM Int. Publ., Metals Park, OH, 1987).
[12] T. B. Massalski, H. Okamoto, P. R. Subrmanian, and L. Kacprzak, *Binary Alloys Phase Diagrams* (ASM Int. Publ., Metals Park, OH, 1990).
[13] A. Markström, D. Andersson, and K. Frisk, CALPHAD: Comput. Coupling Phase Diagrams Thermochem. **32**, 615 (2008).
[14] A. I. Gusev, Phys. Usp. **43**, 1 (2000).
[15] E. M. Fedorov and R. A. Andrievskii, Izv. Akad. Nauk SSSR, Neorg, Mater. **15**, 454 (1979).
[16] A. Zunger, S.-H. Wei, L. G. Ferreira, and J. E. Bernard, Phys. Rev. Lett. **65**, 353 (1990).
[17] K. A. Mäder and A. Zunger, Phys. Rev. B **51**, 10462 (1995).
[18] I. A. Abrikosov, S. I. Simak, B. Johansson, A. V. Ruban, and H. L. Skriver, Phys. Rev. B **56**, 9319 (1997).
[19] C. Jiang, C. Wolverton, J. Sofo, L. Q. Chen, and Z.-K. Liu, Phys. Rev. B **69**, 214202 (2004).
[20] D. Shin, A. van de Walle, Y. Wang, and Z.-K. Liu, Phys. Rev. B **76**, 144204 (2007).
[21] G. M. Stocks, D. M. Nicholson, W. A. Shelton, B. L. Gyorffy, F. J. Pinski, D. D. Johnson, J. B. Staunton, B. Ginatempo, P. E. A. Turchi, and M. Sluiter, in *Statics and Dynamics of Alloy Phase Transformations*, edited by P. E. A. Turchi and A. Gonis, NATO Advanced Studies Institute, Series B: Physics (Plenum Press, New York, 1994), Vol. 319, p. 305.
[22] L. Vitos, I. A. Abrikosov, and B. Johansson, Phys. Rev. Lett. **87**, 156401 (2001).
[23] D. A. Rowlands, A. Ernst, B. L. Gyorffy, and J. B. Staunton, Phys. Rev. B **73**, 165122 (2006).
[24] A. V. Ruban, S. I. Simak, S. Shallcross, and H. L. Skriver, Phys. Rev. B **67**, 214302 (2003).
[25] A. E. Kissavos, S. Shallcross, L. Kaufman, O. Granas, A. V. Ruban, and I. A. Abrikosov, Phys. Rev. B **75**, 184203 (2007).
[26] B. Alling, A. V. Ruban, A. Karimi, O. E. Peil, S. I. Simak, L. Hultman, and I. A. Abrikosov, Phys. Rev. B **75**, 045123 (2007).
[27] J. M. Sanchez, F. Ducastelle, and D. Gratias, Physica A **128**, 334 (1984).
[28] D. de Fontaine, Solid State Phys. **47**, 33 (1994).
[29] A. Zunger, in *Statics and Dynamics of Alloy Phase Transformations*, edited by P. E. Turchi and A. Finel, NATO Advanced Studies Institute, Series B: Physics (Plenum Press, New York, 1994), Vol. 319, p. 361.
[30] G. L. W. Hart, V. Blum, M. J. Walorski, and A. Zunger, Nature Mater. **4**, 391 (2005).
[31] A. van de Walle, G. Ghosh, and M. Asta, in *Applied Computational Materials Modeling: Theory, Simulation and Experiment*, edited by G. Bozzolo, R. D. Noebe, and P. Abel (Springer, New York, 2007), pp. 1–34.
[32] A. van de Walle and G. Ceder, J. Phase Equilib. **23**, 348 (2002).
[33] A. van de Walle, M. Asta, and G. Ceder, CALPHAD: Comput. Coupling Phase Diagrams Thermochem. **26**, 539 (2002).
[34] A. van de Walle and M. Asta, Modell. Simul. Mater. Sci. Eng. **10**, 521 (2002).
[35] B. P. Burton and A. Van de Walle, Phys. Chem. Miner. **30**, 88 (2003).
[36] B. P. Burton and A. van de Walle, Chem. Geol. **225**, 222 (2006).
[37] B. P. Burton and A. van de Walle, J. Appl. Phys. **100**, 113528

(2006).
[38] B. P. Burton and T. Nishimatsu, Appl. Phys. Lett. **91**, 092907 (2007).
[39] J. Z. Liu, G. Ghosh, A. van de Walle, and M. Asta, Phys. Rev. B **75**, 104117 (2007) .
[40] G. Ghosh, A. van de Walle, and M. Asta, Acta Mater. **56**, 3202 (2008).
[41] G. Kresse and J. Hafner, Phys. Rev. B **47**, 558 (1993); **49**, 14251 (1994); G. Kresse and J. Furthmüller, Comput. Mater. Sci. **6**, 15 (1996); Phys. Rev. B **54**, 11169 (1996); cf. http://tph.tuwien.ac.at/vasp/guide/vasp.html
[42] D. Vanderbilt, Phys. Rev. B **41**, 7892 (1990).
[43] J. P. Perdew, K. Burke, and M. Ernzerhof, Phys. Rev. Lett. **77**, 3865 (1996); **78**, 1396(E) (1997).
[44] A. van de Walle and G. Ceder, Rev. Mod. Phys. **74**, 11 (2002).
[45] E. J. Wu, G. Ceder, and A. van de Walle, Phys. Rev. B **67**, 134103 (2003).
[46] R. D. Shannon and C. T. Prewitt, Acta Crystallogr., Sect. B: Struct. Crystallogr. Cryst. Chem. **25**, 925 (1969).
[47] L. G. Ferreira, A. A. Mbaye, and A. Zunger, Phys. Rev. B **35**, 6475 (1987).
[48] A. Zunger, S.-H. Wei, A. A. Mbaye, and L. G. Ferreira, Acta Metall. Mater **36**, 2239 (1988).
[49] L. G. Ferreira, A. A. Mbaye, and A. Zunger, Phys. Rev. B **37**, 10547 (1988).
[50] B. P. Burton, N. Dupin, S. G. Fries, G. Grimvall, A. Fernández Guillermet, P. Miodownik, W. A. Oates, and V. Vinograd, Z. Metallkd. **92**, 514 (2001).